IEEE Access
Multidisciplinary | Rapid Review | Open Access Journal

Received August 24, 2018, accepted October 1, 2018, date of publication October 30, 2018,
date of current version November 19, 2018.

Digital Object Identifier 10.1109/ACCESS.2018.2875411

A Parametric Study of a Pilot Solar Chimney Power Plant Using CFD

EHSAN GHOLAMALIZADEH AND JAE DONG CHUNG
Department of Mechanical Engineering, Sejong University, Seoul 05006, South Korea

Corresponding author: Jae Dong Chung (jdchung@sejong.ac.kr)

This work was supported by the Korea Institute of Energy Technology Evaluation and Planning (KETEP) and the Ministry of Trade, Industry & Energy (MOTIE) of the Republic of Korea (No. 20172010105570).

ABSTRACT Using preliminary evaluations, a pilot solar chimney power plant with a 1-kW nominal power output was designed and built in Kerman City, Iran. This power plant produced about 400-W electrical power at high solar irradiance, which was 60% less than its nominal potential capacity. This investigation simulated fluid flow and heat transfer characteristics through this pilot, using ANSYS Fluent. The model was validated by comparing the results with the measured data of the Kerman pilot power plant. Then, parametric studies were performed to improve the main configurations of the system. The configuration of the system was improved by considering the collector and chimney dimensions. The collector inlet and outlet heights were re-designed, and then, the system was scaled at the factors of 1, 1.5, 3, and 5 in the radial direction, with three chimney heights of 60, 90, and 120 m. It was found that the collector of the Kerman pilot reached its maximum efficiency when its height was increased from 1 m at the collector inlet to 2 m at the collector outlet. Finally, a configuration to produce a power output of 1 kW was determined, with a scale factor of 1.5. More investigations to improve the system performance were conducted, and the velocity and temperature distributions for configurations with a scale factor of 3 at three different chimney heights were illustrated.

INDEX TERMS Renewable energy, solar thermal system, solar chimney power plant, Kerman pilot power plant, CFD analysis.

I. INTRODUCTION

A solar chimney power plant (SCPP) is a type of solar thermal power system which collects both direct and diffuse solar radiation to convert thermal energy into electricity. A conventional SCPP has four main parts: a solar collector; a tower called a chimney, which is located at the center of the solar collector; the ground, which is generally used as the energy storage media; and a wind turbine. The solar collector and the ground are covered by a semi-transparent roof, typically made of glass. Short-wavelength solar radiation can freely pass through the collector's roof and then is absorbed by the storage media, which causes an increase in the temperature of its surface. Because the radiation emitted from the ground surface is in the long wavelength radiation range, the collector roof is practically opaque to the emitted radiation. Consequently, the heat trapped by the solar collector causes the temperature inside the collector to increase (the greenhouse effect). As the air beneath the collector becomes warmer, its density decreases and as a result, the air inside the collector becomes lighter than the air inside the chimney. Accordingly, its upward buoyancy forced through the chimney produces a continuous updraft. To convert the energy available in the airflow into mechanical energy a wind turbine is installed at the chimney base and finally, a generator converts the mechanical energy into electricity. A prototype SCPP was built in Manzanares, Spain, in 1982, with a nominal output capacity of 50 kW and was tested for seven years [1]. The Manzanares prototype had a collector with a radius and mean height of 122 m and 1.85 m, respectively. The diameter and height of its chimney were 10 m and 194.6 m, respectively, and a wind turbine was installed at its base.

The theoretical modeling and test results of the Manzanares prototype reported by Haaf *et al.* [2] and Haaf [3] demonstrated the feasibility of the SCPP concept. Since then, investigations on the performance of the SCPP systems have been widely carried out [4]–[18]. The first computational fluid dynamics (CFD) code using the finite volume method, which was developed by Bernardes *et al.* [19], solves the Navier-Stokes and energy equations in the steady state for

a natural laminar convection. Afterward, Pastohr *et al.* [20] employed a commercial CFD package to simulate a solar chimney. In recent years, the use of commercial CFD packages to analyze fluid flow and heat transfer in SCPP systems has widely increased. Most of the first attempts were carried out in a 2-D Axisymmetric system. However, in 2-D models, the CFD packages are limited to modeling an opaque medium. Hence, in those investigations some non-physical boundary conditions were imposed to model heat transfer inside the collector. In [20]–[23], a uniform heat source within the air, a heat source for the thin ground layer, specific wall temperatures or heat fluxes were developed in 2-D Axisymmetric modeling. Recently, in [24]–[28], 3-D CFD models were developed which simulated a semi-transparent medium for the collector roof. In [29], a comprehensive updated review including the experimental, analytical and numerical investigations of the solar chimney applications was presented. To study the feasibility of SCPP systems in the central desert areas of Iran, a pilot was built in Kerman City (Fig. 1) with a nominal power output of 1kW. The Kerman pilot had a chimney with a height and diameter of 60 m and 3 m, respectively. Its solar collector was covered with a single glazed roof with a radius and a mean height of 20 m and 2m, respectively. This pilot could only produce about 400 Watts at its highest power output production.

FIGURE 1. Kerman pilot solar chimney power plant.

This study investigates the fluid flow and heat transfer characteristics of the Kerman pilot system using ANSYS Fluent. Then, to improve its performance, a parametric study is performed on the dimensional parameters of the Kerman pilot. The system performance is analyzed by accurate calculations of the collector and chimney efficiencies using the CFD results.

II. GEOGRAPHICAL CHARACTERISTICS OF THE KERMAN CITY REGION

Kerman is a sunny city located in the central region of Iran (latitude 30ř 17' North and longitude 57ř 5' East) surrounded by desert areas. The average solar irradiation in Kerman City is more than 2000 kWh/m^2 year and the number of solar hours in this area is almost 2800 hours in a year [30]. Hence, the potential electrical power that can be produced by solar energy in this region is high. On the other hand, the extreme deficit of water in these desert areas is a major limitation when it comes to constructing conventional thermal power stations, which need an abundant water supply. Unlike conventional power stations, and some other solar thermal power station types, SCPPs do not need cooling water, an advantage which was key to the decision to build this type of solar technology in Kerman City. The SCPP technology is one of the most promising and practical ways to produce electricity from solar energy in these conditions.

III. NUMERICAL PROCEDURE, COMPUTATIONAL DOMAIN, AND BOUNDARY CONDITIONS

To simulate the fluid flow and heat transfer through the system, the steady-state conservation equations of mass, momentum, and energy coupled to the radiative-transfer equation were solved using the Commercial CFD package ANSYS Fluent 15 [31]. The governing equations for turbulent flow are listed as below:

Continuity Equation:

$$\frac{\partial}{\partial x_i}(\rho u_i) = 0 \tag{1}$$

Momentum Equation:

$$\frac{\partial}{\partial x_j}\left(\rho u_i u_j\right) = -\frac{\partial p}{\partial x_i} + \frac{\partial}{\partial x_j}(-\rho\overline{u_i' u_j'}) + \frac{\partial}{\partial x_j}\left[\mu\left(\frac{\partial u_i}{\partial x_j} + \frac{\partial u_j}{\partial x_i} - \frac{2}{3}\delta_{ij}\frac{\partial u_l}{\partial x_l}\right)\right] + \rho\vec{g} \tag{2}$$

The energy equation is defined as follow:

$$\nabla \cdot (\vec{v}(\rho E + p)) = \nabla \cdot \left(\mathrm{k}_{eff}\nabla \mathrm{T} - \sum_j h_j \vec{J}_j + (\bar{\bar{\tau}}_{eff} \cdot \vec{v})\right) + S_h \tag{3}$$

To evaluate the strength of the buoyancy-driven flow through the system the Rayleigh number is calculated. Because the Rayleigh number was within the turbulent regime (Ra $> 10^{10}$), the turbulent flow was simulated using the RNG k-ε turbulence closure. Scalable wall functions were employed for the near-wall treatment to simulate the turbulent model in the boundary layer. The Boussinesq approximation was used to simulate the buoyancy-driven flow. The reverse fan interior boundary condition was simulated to account for the pressure drop across the turbine at the chimney base.

The Discrete Ordinates (Do) radiation model is able to simulate radiation through a semi-transparent collector roof with non-grey radiation behavior. Therefore, this model was chosen to discretize the radiative transfer equation integrated

to each wavelength band $\Delta\lambda$ which were assumed to be grey. The radiative transfer equation is described as follow:

$$\nabla \cdot (I_\lambda(\vec{r},\vec{s})\vec{s}) + (a_\lambda + \sigma_s) I_\lambda(\vec{r},\vec{s}) = a_\lambda n^2 I_{by} + \frac{\sigma_s}{4\pi}\int_0^{4\pi} I_\lambda(\vec{r},\vec{s}')\varphi(\vec{s},\vec{s}')d\Omega' \quad (4)$$

The solar ray-tracing algorithm of the solar model was employed to calculate the direct illumination energy source resulting from the incident solar radiation. The wavelength of the solar radiation received by the collector roof is within the range of 0.29 to 2.5 μm [32]. The collector is covered by a semi-transparent roof that has high transmittance through the visible solar band, but low infrared transmittance. The optical properties (absorptivity and transmissivity) of the collector roof medium (e.g. glass) were separated into different bands including a visible band ($0.38 < \lambda < 0.78$ μm) and an infrared ($\lambda > 0.78$ μm) band.

The geometric parameters of the Kerman pilot SCPP are as follows: they include a collector radius of 20 m, a collector mean height of 2 m covered by single-glazed glass, a chimney diameter of 3 m, and a chimney height of 60 m. To simulate this system, a three-dimensional structured mesh with refined grids near the walls was adopted (Fig. 2).

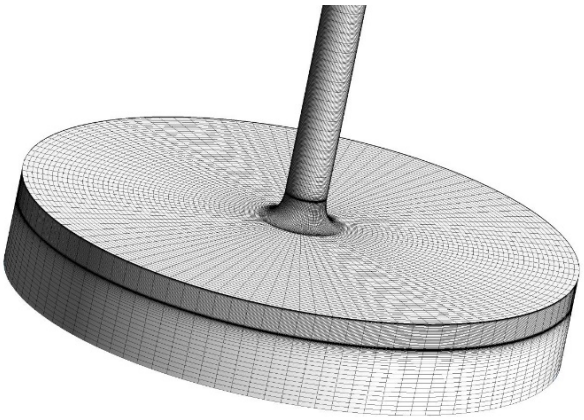

FIGURE 2. Structured meshes of the system computational domain.

A mesh study was performed to obtain grid independent solutions, using three different mesh sizes. To verify the solution insensitivity, the mass flow rate of the system and the temperature rise through the collector were captured. The hexahedral fine cell sizes in the flow direction were in the range of 0.05 m to 0.2 m. The number of grid elements inside the computational domain was about 1,300,000. Details about the relative differences in the results for the coarse and intermediate meshes and the fine mesh are shown in Table 1.

The thickness of the ground in the computational domain was set to 5 m, and the bottom temperature was set as the ambient temperature. The glazed roof of the collector was modeled as a semi-transparent medium and the convection and solar radiation were set as the roof boundary conditions.

TABLE 1. Deviation in simulation results for coarser and intermediate meshes from the fine mesh.

	Mass flow rate	Collector temperature rise
Coarse mesh	8.4%	9.7%
Intermediate mesh	1.8%	2.9%

The pressure inlet and pressure outlet were set to the collector inlet and the chimney outlet, respectively, for which, the values were set to 0 Pa to simulate the buoyancy-driven flow through the system. To model the turbine at the chimney base the reverse fan interior boundary condition was modeled, and the value of the pressure jump was calculated using an iterative approach [25]. The turbine efficiency of the system was assumed to be 0.8. The external chimney surface was assumed to be an adiabatic wall. The pressure-based coupled algorithm was adopted to solve the coupled systems of the equations.

IV. THE SYSTEM PERFORMANCE CALCULATION

The numerical results obtained by the CFD approach were used to evaluate the system performance. The collector efficiency is calculated as the ratio of the enthalpy rise inside the collector to the entrance solar energy, as given below:

$$\eta_{coll} = \frac{\dot{m}\Delta h}{GA_{coll}} \quad (5)$$

where Δh stands for the airflow enthalpy increase through the collector. The chimney efficiency is defined as follows:

$$\eta_c = \frac{g H_c}{C_p T_{amp}} \quad (6)$$

Then, the total efficiency and the power output of the SCPP can be calculated by the following equations:

The Total Efficiency:

$$\eta_{SCPP} = \eta_{coll}\eta_c\eta_t\eta_{gen} \quad (7)$$

The power output:

$$P_{SCPP} = \eta_{SCPP} G A_{coll} \quad (8)$$

V. RESULTS AND DISCUSSION

The fluid flow and heat transfer characteristics of the Kerman pilot SCPP were considered. The solar irradiation which enters through the collector roof into the computational area was calculated using the Solar Load Model of ANSYS Fluent taking into account the time, date, and geographical location of the site. The simulations were conducted at midday on June 21th when the solar irradiation was 882 W/m^2. The model used to simulate the system was validated by comparing the results with the measured data of the Kerman pilot SCPP. The measured mass flow rate and collector efficiency of the Kerman pilot power plant in the loaded condition were about 28.5 kg/s and 24.4 %, respectively. The numerical model predicted the mass flow rate of 29.33 kg/s and, the collector efficiency of 25.9%, which are in close agreements

TABLE 2. Mass flow rate, temperature rise and enthalpy change in the Kerman pilot.

	No-load condition	Loaded condition
Mass flow rate (kg/s)	38.73	29.33
Temperature rise (K)	7.79	9.28
Collector efficiency [-]	28.7 %	25.9 %

with the measured data of the Kerman pilot SCPP. Moreover, the numerical model predicted a power output of about 430 Watts, which is in a good agreement with the measured electrical power of 400 Watts produced by the Kerman pilot SCPP at its highest performance. The simulations were conducted under two different conditions: the no-load condition (no-turbine set up) and the loaded condition (during turbine operation).

A. FLUID FLOW AND HEAT TRANSFER OF THE KERMAN PILOT

1) DISTRIBUTION OF VELOCITY

The velocity distributions through the Kerman pilot under two different conditions, the no-load and loaded conditions, are illustrated in Fig. 3. The influence of the turbine operation on the velocity distribution inside the Kerman pilot can be evaluated by comparing Figs. 3.a and 3.b. The average velocity at the turbine base in the no-load condition is about 5.09 m/s, while it reaches 3.86 m/s in the loaded condition. It can be seen that the turbine operation has a significant effect on the airflow.

The main reason is that the pressure drop across the turbine creates a drag force against the flow which causes a significant reduction in the mass flow rate. Moreover, the airflow reaches its maximum velocity at the chimney base.

2) DISTRIBUTION OF TEMPERATURE

Fig. 4 shows the temperature distributions through the airflow and inside the energy storage media in the Kerman pilot for the no-load and loaded conditions. Comparing Figs. 4.a and 4.b, it can be seen that when the turbine operates change of the airflow temperature increases in the collector. The main reason for this is that, in the loaded condition the mass flow rate decreases, and the average time that the air remains inside the collector increases, and therefore, the air inside the collector is heated more, compared to the no-load condition. That is, the mass flow rate of the system in the loaded condition is lower. Hence, the enthalpy change through the collector in the loaded condition is affected by two significant parameters, which are an increase in the temperature rise in the collector and a decrease in the mass flow rate.

Table 2 compares the mass flow rate, temperature rise, and collector efficiency of the Kerman pilot in the no-load and loaded conditions. It was found that the collector efficiency in the loaded condition was lower than in the no-load condition. The measured mass flow rate and collector efficiency

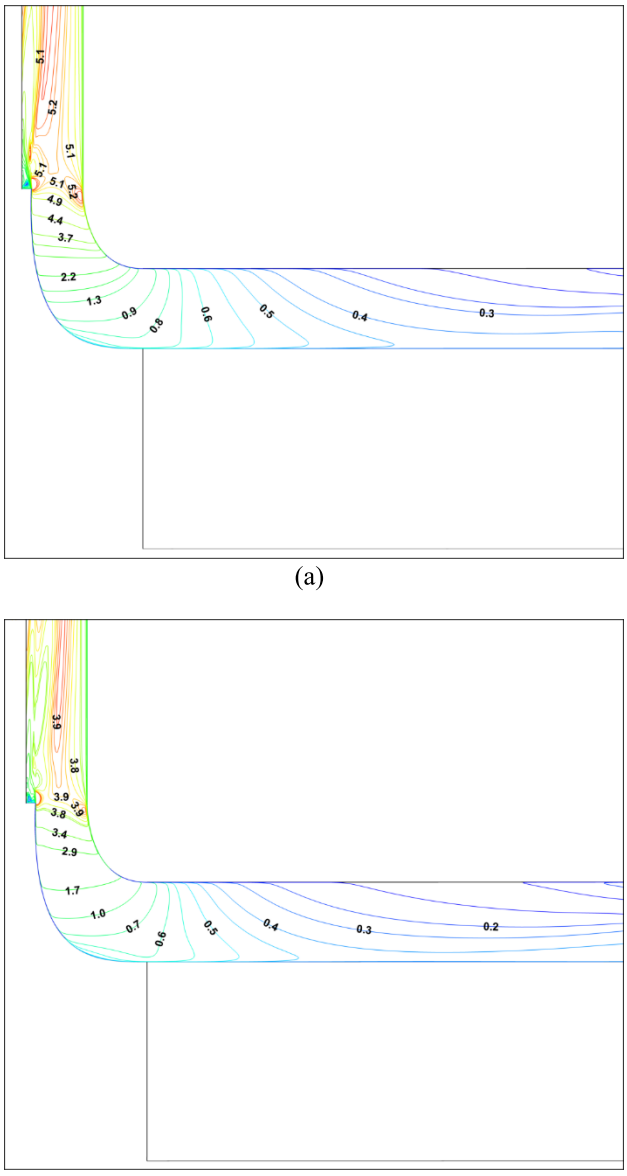

FIGURE 3. Velocity (m/s) distribution through the Kerman pilot in the no-load (3.a) and loaded (3.b) conditions.

of the system in the loaded condition were about 28.5 kg/s and 24.4 %, respectively.

B. PARAMETRIC STUDY

To develop the performance of the Kerman pilot, a number of parametric studies on its geometrical parameters were performed. These parameters included the inlet and outlet collector heights, the collector radius, and the chimney height and the chimney diameter.

1) CONFIGURATION OF THE SOLAR COLLECTOR

First, the configuration of the collector was considered. The flat collector of the Kerman pilot had a height of 2m (H1 = H2 = 2m). A parametric study on the roof inclination was performed by setting the inlet collector height (H1) and

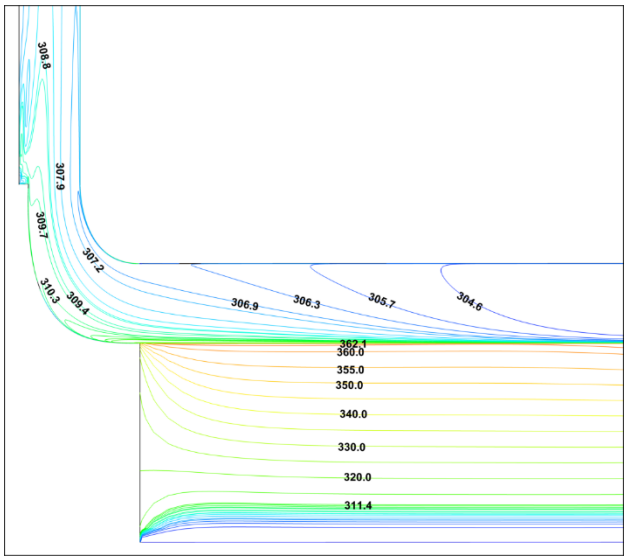

(a)

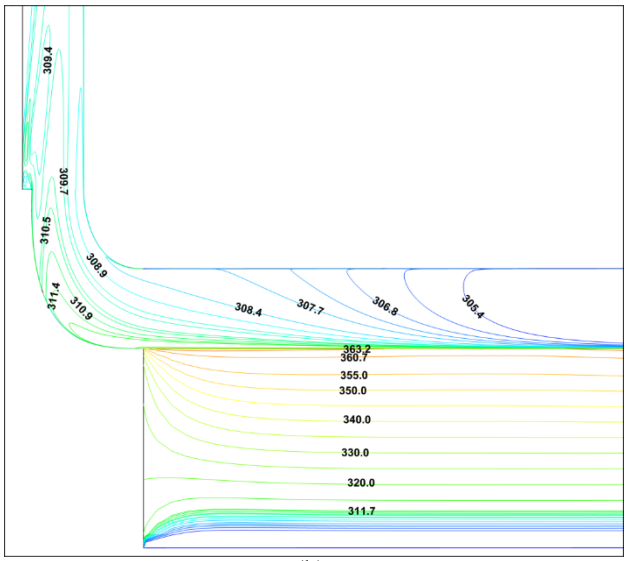

(b)

FIGURE 4. Temperature (K) distribution through the Kerman pilot in the no-load (4.a) and loaded (4.b) conditions.

the outlet collector height (H2). H1 was fixed to three different values; 0.5m, 1m, and 1.5m. Then, for each case, the roof inclination was adjusted by increasing H2 from the value of H1 to 2m with a step of 0.5m. Hence, 10 different configurations with respect to the collector radius as well as other structural parameters of the Kerman pilot were considered.

Fig. 5 shows the collector efficiency for each case in loaded condition. The Kerman pilot collector efficiency reached its maximum value when H1 and H2 were 1m and 2m, respectively. Hence, this configuration was selected to develop the Kerman pilot performance.

2) SCALING THE CONFIGURATION OF THE KERMAN PILOT

To perform a parametric study, the collector radius and the chimney diameter of the system were scaled in the radial

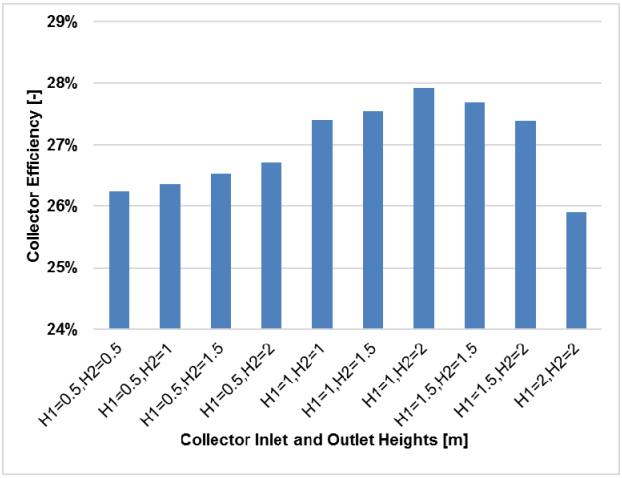

FIGURE 5. Collector efficiency for different inclined collector configurations of the Kerman pilot in loaded condition.

direction when the chimney heights were fixed to 60m, 90m, and 120m. Simulations were conducted by implementing different scale factors (SF), of 1, 1.5, 3, and 5. Altogether, 12 different configurations were studied and compared. However, it should be mentioned that for obtaining an optimal SF, an optimization approach to find an optimal chimney diameter can be conducted [7].

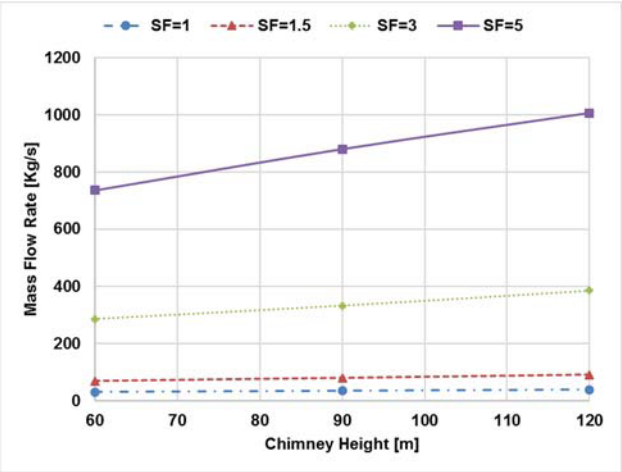

FIGURE 6. Mass flow rate of the scaled configurations.

The mass flow rates of these configurations are shown in Fig. 6. It can be seen that smaller power plants are not able to produce a high mass flow. Moreover, at a small SF value, the mass flow rate increases slightly when the chimney height is increased. In contrast, at a higher SF value, an increase in the chimney height causes a notable increase in the mass flow.

Fig. 7 shows the power output for any simulated configuration. It can be observed that the diagrams of the power output have the same trend as those for the mass flow rate. The maximum obtained power output of a system with the SF value of 1 (corresponding to a system with the same collector

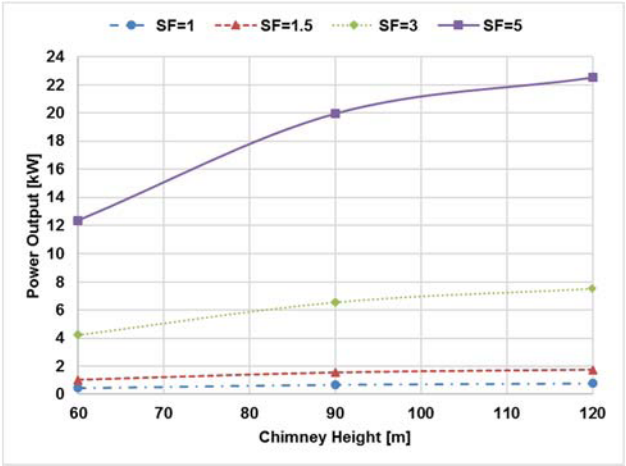

FIGURE 7. Power output of the scaled configurations.

and chimney diameter as the Kerman Pilot, and different chimney heights) reaches 0.78kW when the chimney height is increased to 120m. Hence, it was found that a system with SF=1 is not able to produce 1 kilowatt power output only by increasing the chimney height with respect to its range. Hence, the system was scaled in the radial direction with an SF of 1.5. For this case, the power output increases from 1kW to 1.75kW when the chimney height is increased from 60m to 120m. Moreover, according to Fig. 7, at higher SF values, the power output increases at a higher rate when the chimney height is increased.

3) CFD SIMULATION RESULTS

The preliminary goal for building the Kerman pilot was to study on the feasibility of an SCPP in the desert area of Iran. Hence, the Kerman pilot was designed to produce 1kW power. However, in actuality the Kerman pilot was only able to produce 400 Watts electrical power at its highest performance, which was 60% less than its nominal potential capacity. The numerical model also predicted a power output of about 430 Watts.

In previous sections, the performance of the Kerman pilot was considered, and then, a parametric study to improve its performance was performed. According to Fig. 7, a system with an SF of 1.5 and a chimney height of 60m (the same chimney height as the Kerman pilot) should be able to produce a power output of 1kW. The velocity and temperature distributions through this system in loaded condition are illustrated in Figs. 8.a and 8.b, respectively. The airflow reaches an average velocity of 4.06 m/s at the chimney base.

Next, simulations with an SF of 3 at the three chimney heights in loaded condition were performed. The velocity distributions through the systems with the simulated configurations are illustrated in Fig. 9. The average velocity at the chimney base increases from 4.24 m/s to 5.73 m/s when the chimney height is increased from 60 m to 120 m.

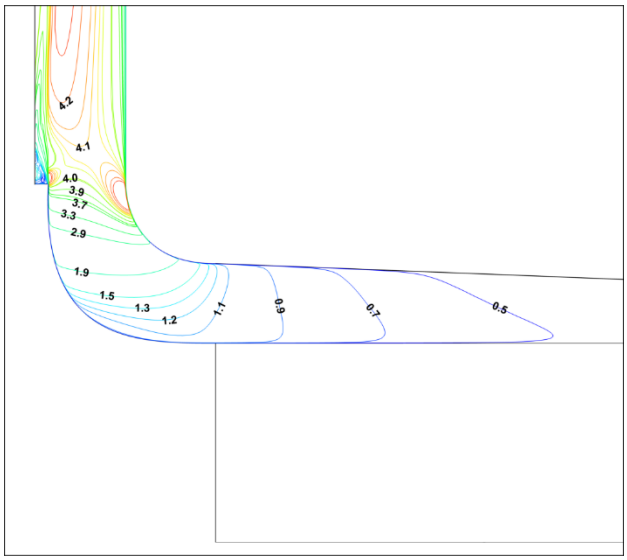

(a)

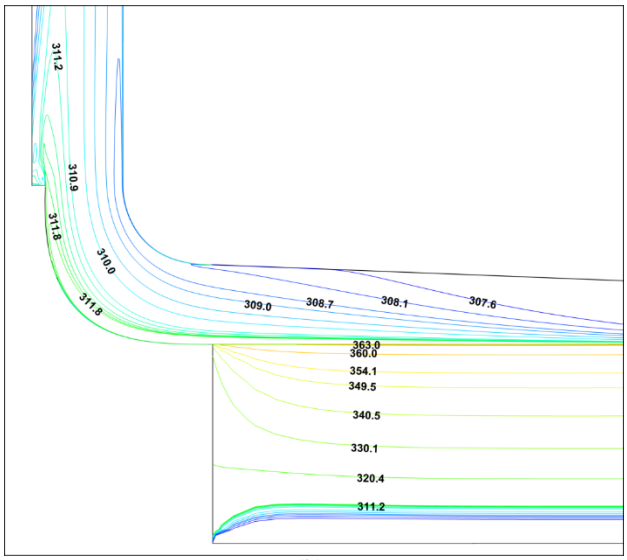

(b)

FIGURE 8. Velocity (m/s) (8.a) and temperature (K) (8.b) distributions through a system with an SF of 1.5 and chimney height of 60m in the loaded condition.

Fig. 10 shows the temperature distributions for the corresponding configurations. In a system with a higher chimney height, in which the mass flow rate is higher, the average heating time of the airflow through the collector is lower, which results in a decrease in the collector temperature rise. Hence, an increase in the chimney height causes an increase in the mass flow rate on the one hand, but a decrease in temperature rise through the collector on the other hand.

To investigate the effect of the tradeoff between the mass flow rate and temperature rise on the collector efficiency, the efficiencies of the systems were calculated for three different chimney heights. The values of the collector efficiencies were 28.61%, 29.54%, and 29.03% while the chimney heights were 60m, 90m, and 120m, respectively. It was found

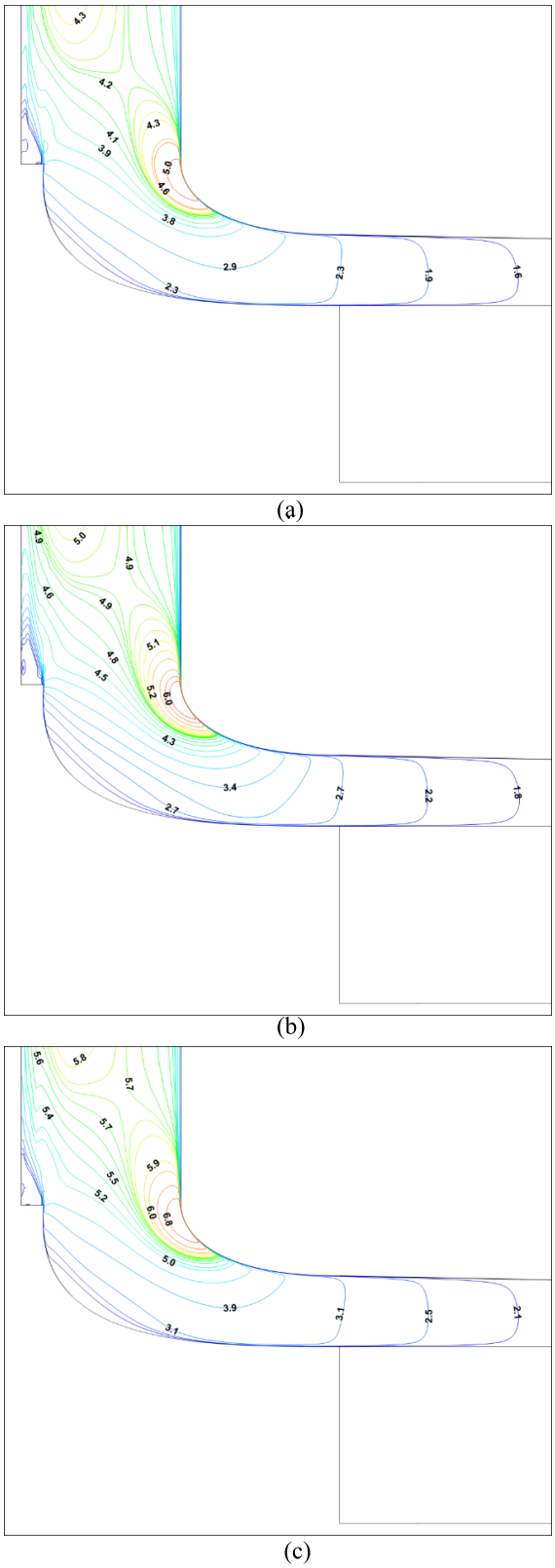

FIGURE 9. Velocity distributions (m/s) through systems with an SF of 3 and chimney heights of 60m (9.a), 90m (9.b), and 120m (9.c) in the loaded condition.

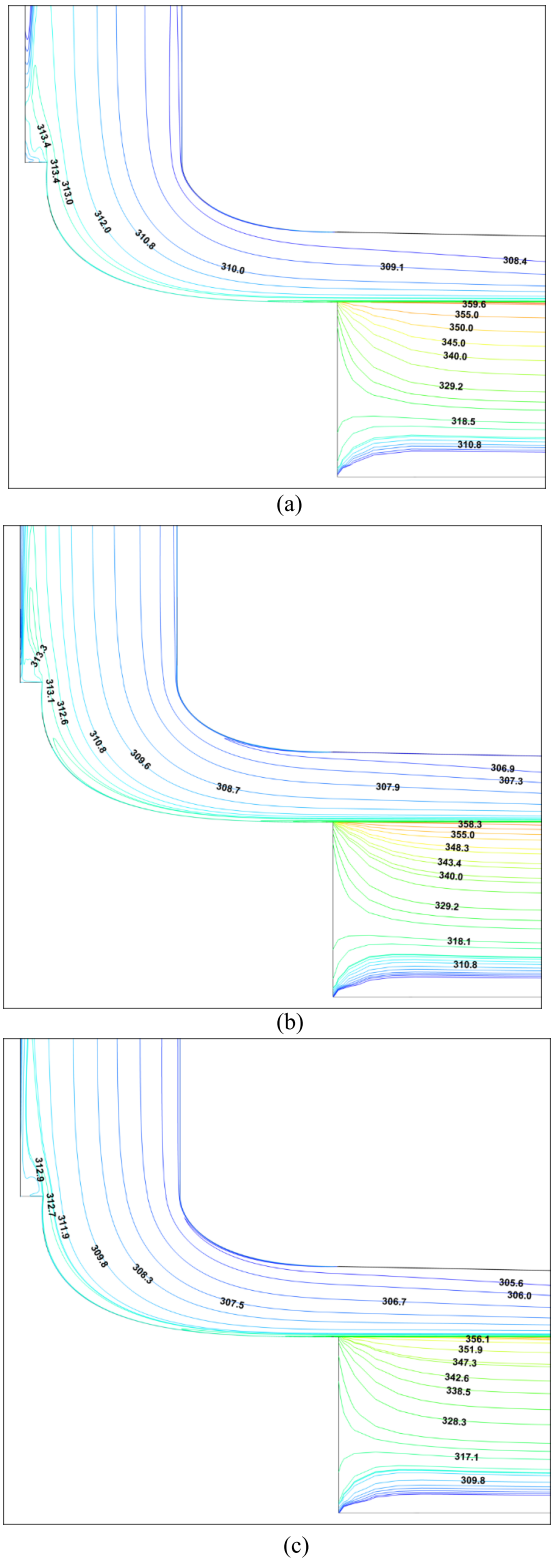

FIGURE 10. Temperature (K) distributions through systems with an SF of 3 and chimney heights of 60m (10.a), 90m (10.b), and 120m (10.c) in the loaded condition.

that the increase in the chimney height from 60m to 90m causes an increase in the collector efficiency, which shows that the effect of the mass flow rate on the increase in enthalpy rise inside the collector is dominant, compared to the effect of a decrease in temperature rise resulting from a decrease in the enthalpy rise. An increase in the chimney height from 90m to 120m causes a drop in collector efficiency.

VI. CONCLUSIONS

In this paper, first, the fluid flow and heat transfer characteristics of a pilot solar chimney built in Kerman City, Iran were simulated using CFD. Because the operating capacity of this pilot was lower than the initially expected performance, which was 1kW power output, a parametric study to improve its performance was performed.

First, the configuration of the inclined solar collector was considered by changing its inlet and outlet heights. Then, other main parameters including the collector radius, and the chimney height and diameter were taken into account by scaling the structural configuration of the Kerman pilot. The pilot was scaled with SFs of 1, 1.5, 3, and 5 in the radial direction at three chimney heights, of 60m, 90m, and 120m. The results showed that the Kerman pilot collector gained its maximum performance when its height was increased from 1m at the collector inlet to 2m at the collector outlet. Therefore, this configuration was selected to improve the Kerman pilot performance. Moreover, the mass flow rate and power output were determined for different scaled configurations. It was found that the existing configuration of the Kerman pilot, corresponding to an SF value of 1, was not able to produce the expected power output when the chimney height was increased from 60m to 120m.

However, a power output of about 1kW was obtained with an SF of 1.5. In addition, velocity and temperature distributions for the configurations with an SF of 3 at three chimney heights were illustrated. It can be concluded that the methodology presented in this investigation is applicable to the design of an SCPP system.

NOMENCLATURE

A	area (m2)
a_λ	spectral absorption coefficient
C_p	specific heat capacity (J/kg.K)
E	energy (J)
G	solar irradiation (W/m2)
g	gravitational acceleration (m/s2)
h	species enthalpy(energy/mass)
I	radiation intensity (W/m2) J diffusion flux (kg/m2s)
k	thermal conductivity (W/m.K) m mass flow rate (kg/m3)
n	refractive index
P	power (W)
p	pressure (Pa)
r	radial coordinate (m)
s	direction
S_h	heat source term
T	temperature (K) u velocity magnitude (m/s)
ν	velocity (m/s)
x	axial coordinate (m)
Δ	differential
η	efficiency
λ	wavelength (μm)
μ	dynamic viscosity (Pa-s)
ρ	density (kg/m3)
σ_S	Scattering coefficient (1/m)
τ	Stress tensor (Pa)
φ	phase function
Ω	solid angle (radians)

Subscripts

amb	ambient
b	black body
c	chimney
coll	collector
eff	effective
gen	generator
SCPP	solar chimney power plant
t	turbine

REFERENCES

[1] J. Schlaich, *The Solar Chimney: Electricity From the Sun*. Stuttgart, Germany: Edition Axel Menges, 1995.

[2] W. Haaf, K. Friedrich, G. Mayr, and J. Schlaich, "Solar chimneys part I: Principle and construction of the pilot plant in manzanares," *Int. J. Solar Energy*, vol. 2, no. 1, pp. 3–20, 1983.

[3] W. Haaf, "Solar chimneys: Part II: Preliminary test results from the manzanares pilot plant," *Int. J. Solar Energy*, vol. 2, no. 2, pp. 141–161, 1984.

[4] M. A. dos Santos Bernardes, T. W. Von Backström, and D. G. Kröger, "Analysis of some available heat transfer coefficients applicable to solar chimney power plant collectors," *Solar Energy*, vol. 83, no. 2, pp. 264–275, 2009.

[5] M. A. dos Santos Bernardes, A. Voß, and G. Weinrebe, "Thermal and technical analyses of solar chimneys," *Solar Energy*, vol. 75, no. 6, pp. 511–524, 2003.

[6] Y. J. Dai, H. B. Huang, and R. Z. Wang, "Case study of solar chimney power plants in Northwestern regions of China," *Renew. Energy*, vol. 28, no. 8, pp. 1295–1304, 2003.

[7] E. Gholamalizadeh and M.-H. Kim, "Thermo-economic triple-objective optimization of a solar chimney power plant using genetic algorithms," *Energy*, vol. 70, no. 1, pp. 204–211, 2014.

[8] E. Gholamalizadeh and S. H. Mansouri, "A comprehensive approach to design and improve a solar chimney power plant: A special case–Kerman project," *Appl. Energy*, vol. 102, pp. 975–982, Feb. 2013.

[9] M. O. Hamdan, "Analysis of a solar chimney power plant in the Arabian Gulf region," *Renew. Energy*, vol. 36, no. 10, pp. 2593–2598, 2011.

[10] S. Larbi, A. Bouhdjar, and T. Chergui, "Performance analysis of a solar chimney power plant in the southwestern region of Algeria," *Renew. Sustain. Energy Rev.*, vol. 14, no. 1, pp. 470–477, 2010.

[11] M. Mehrpooya, M. Shahsavan, and M. M. M. Sharifzadeh, "Modeling, energy and exergy analysis of solar chimney power plant-Tehran climate data case study," *Energy*, vol. 115, pp. 257–273, Nov. 2016.

[12] S. Nizetic, N. Ninic, and B. Klarin, "Analysis and feasibility of implementing solar chimney power plants in the Mediterranean region," *Energy*, vol. 33, no. 11, pp. 1680–1690, 2008.

[13] N. Pasumarthi and S. A. Sherif, "Experimental and theoretical performance of a demonstration solar chimney model—Part I: Mathematical model development," *Int. J. Energy Res.*, vol. 22, no. 3, pp. 277–288, 1998.

[14] J. P. Pretorius and D. G. Kröger, "Solar chimney power plant performance," *J. Solar Energy Eng.*, vol. 128, no. 3, pp. 302–311, 2006.

[15] X. Zhou, F. Wang, J. Fan, and R. M. Ochieng, "Performance of solar chimney power plant in Qinghai-Tibet Plateau," *Renew. Sustain. Energy Rev.*, vol. 14, no. 8, pp. 2249–2255, 2010.

[16] X. Zhou, J. Yang, B. Xiao, G. Hou, and F. Xing, "Analysis of chimney height for solar chimney power plant," *Appl. Thermal Eng.*, vol. 29, no. 1, pp. 178–185, 2009.

[17] X. Zhou, J. Yang, B. Xiao, and G. Hou, "Experimental study of temperature field in a solar chimney power setup," *Appl. Thermal Eng.*, vol. 27, nos. 11–12, pp. 2044–2050, 2007.

[18] E. Gholamalizadeh and M.-H. Kim, "Multi-objective optimization of a solar chimney power plant with inclined collector roof using genetic algorithm," *Energies*, vol. 9, no. 11, p. 971, 2016.

[19] M. A. dos Santos Bernardes, R. M. Valle, and M. F.-B. Cortez, "Numerical analysis of natural laminar convection in a radial solar heater," *Int. J. Thermal Sci.*, vol. 38, no. 1, pp. 42–50, 1999.
[20] H. Pastohr, O. Kornadt, and K. Gürlebeck, "Numerical and analytical calculations of the temperature and flow field in the upwind power plant," *Int. J. Energy Res.*, vol. 28, no. 6, pp. 495–510, 2004.
[21] A. Koonsrisuk and T. Chitsomboon, "Partial geometric similarity for solar chimney power plant modeling," *Solar Energy*, vol. 83, no. 9, pp. 1611–1618, 2009.
[22] A. Koonsrisuk and T. Chitsomboon, "A single dimensionless variable for solar chimney power plant modeling," *Solar Energy*, vol. 83, no. 12, pp. 2136–2143, 2009.
[23] G. Xu, T. Ming, Y. Pan, F. Meng, and C. Zhou, "Numerical analysis on the performance of solar chimney power plant system," *Energy Convers. Manage.*, vol. 52, no. 2, pp. 876–883, 2011.
[24] P. Guo, J. Li, Y. Wang, and Y. Liu, "Numerical analysis of the optimal turbine pressure drop ratio in a solar chimney power plant," *Solar Energy*, vol. 98, pp. 42–48, Dec. 2013.
[25] E. Gholamalizadeh and M.-H. Kim, "Three-dimensional CFD analysis for simulating the greenhouse effect in solar chimney power plants using a two-band radiation model," *Renew. Energy*, vol. 63, pp. 498–506, Mar. 2014.
[26] P.-H. Guo, J.-Y. Li, and Y. Wang, "Numerical simulations of solar chimney power plant with radiation model," *Renew. Energy*, vol. 62, pp. 24–30, Feb. 2014.
[27] E. Gholamalizadeh and M.-H. Kim, "CFD (computational fluid dynamics) analysis of a solar-chimney power plant with inclined collector roof," *Energy*, vol. 107, pp. 661–667, Jul. 2016.
[28] E. Gholamalizadeh and J. D. Chung, "Analysis of fluid flow and heat transfer on a solar updraft tower power plant coupled with a wind turbine using computational fluid dynamics," *Appl. Thermal Eng.*, vol. 126, pp. 548–558, Nov. 2017.
[29] A. B. Kasaeian, S. Molana, K. Rahmani, and D. Wen, "A review on solar chimney systems," *Renew. Sustain. Energy Rev.*, vol. 67, pp. 954–987, Jan. 2017.
[30] E. Gholamalizadeh and J. D. Chung, "Design of the collector of a solar dish-stirling system: A case study," *IEEE Access*, vol. 5, pp. 20754–20762, 2017.
[31] *ANSYS FLUENT 15.0 User's Guide*, Fluent, Boca Raton, FL, USA, 2013.
[32] J. A. Duffie and W. A. Beckman, *Solar Engineering of Thermal Processes*, 4th ed. New York, NY, USA: Wiley, 2013.

EHSAN GHOLAMALIZADEH received the B.S. and M.S. degrees in mechanical engineering from the Shahid Bahonar University of Kerman, Iran, in 2006 and 2011, respectively, and the Ph.D. degree in mechanical engineering from Kyungpook National University, South Korea, in 2016. He has been an Assistant Professor with the Mechanical Engineering Department, Sejong University, Seoul, South Korea, since 2017. His research interests include solar thermal systems, phase change, and multiphase flow.

JAE DONG CHUNG received the B.S. and Ph.D. degrees from Seoul National University in 1990 and 1996, respectively. He is currently a Professor in mechanical engineering from Sejong University. He has authored one book and more than 90 articles. His research interests include thermal energy storage and transport, low temperature cooling, such as desiccant and adsorption cooling, and nano-scale heat transfer.